

The maximum mass ratio of hierarchical mergers may cause the $q-\chi_{\text{eff}}$ correlation

ADITYA VIJAYKUMAR ,¹ AMANDA M. FARAH ,¹ AND MAYA FISHBACH ,¹

¹Canadian Institute for Theoretical Astrophysics, University of Toronto, 60 St George St, Toronto, ON M5S 3H8, Canada

(Dated: January 8, 2026)

ABSTRACT

Regardless of their initial spins, the merger of two roughly equal mass black holes (BHs) produces a remnant BH of dimensionless spin 0.69. Such remnants can merge with other black holes in dense stellar environments and produce hierarchical mergers. Analyzing the latest catalog binary black hole (BBH) mergers from the LIGO-Virgo-KAGRA detectors, we identify a subpopulation with primary spins consistent with such hierarchical mergers. Consistent with astrophysical expectations for mergers of second generation BHs with first generation BHs, we find that this subpopulation has mass ratios below $0.59_{-0.23}^{+0.18}$. We also infer that 19-88% of the BBH population below this mass ratio is consistent with belonging to the hierarchically-merged population. Our results offer a natural explanation for the narrowing of the effective inspiral spin distribution with mass ratio observed in other studies.

Keywords: Gravitational wave sources (677) — Globular Clusters (656) — High Energy astrophysics (739)

1. INTRODUCTION

Under the right conditions, the remnant black holes (BHs) of binary black hole (BBH) mergers can go on to merge with other BHs. Such mergers are referred to as *hierarchical mergers*, and are a natural outcome of dynamical assembly of BBHs in dense stellar systems (C. L. Rodriguez et al. 2019; F. Antonini et al. 2019). Models of dense stellar clusters predict that the most common type of hierarchical mergers involve the merger of a *second-generation* (2G) BH with a *first-generation* (1G) BH, making up $\approx 10\text{--}20\%$ of the total mergers from these environments (e.g., K. Kremer et al. 2020). BBHs involving higher-generation BHs are also predicted, but their rate is suppressed by a factor of at least ≈ 10 compared to the 2G+1G rate. Thus, if the total merger rate of BBHs in dense stellar systems is high, 2G+1G mergers could make up a significant population of systems detected by the LIGO (LIGO Scientific Collaboration et al. 2015), Virgo (F. Acernese et al. 2015) and KAGRA (T. Akutsu et al. 2021) (LVK) detectors.

Hierarchical mergers have clear population predictions that allow them to be straightforwardly distinguished from the larger BBH population (M. Fishbach et al. 2017; D. Gerosa & E. Berti 2017). This is in contrast to most other formation pathways whose population predictions suffer from large theoretical uncertainties (M.

Mapelli 2020; I. Mandel & A. Farmer 2022; I. Mandel & F. S. Broekgaarden 2022). Hierarchical mergers may therefore be the first subpopulation to be confidently identified, even if they should make up a small fraction of the total population. Robust predictions of a hierarchically-merged subpopulation include:

1. Component spin magnitudes peaked near 0.69 (M. Fishbach et al. 2017; D. Gerosa & E. Berti 2017)
2. Isotopically-distributed spin tilts, on account of merging in dense stellar environments (C. L. Rodriguez et al. 2016), and
3. 2G+1G mergers with mass ratios q below ≈ 0.6 (D. Gerosa & E. Berti 2017; C. L. Rodriguez et al. 2019; C. Kimball et al. 2020).

The LVK collaboration recently published two BBH events with parameters that are compatible with these characteristics (A. G. Abac et al. 2025a). This motivates the search for a subpopulation of hierarchical mergers on the population level. Assuming that hierarchical (2G+1G) mergers follow a primary spin magnitude distribution peaked at $\chi_1 \approx 0.69$ and isotropic spin tilts, we fit for the maximum mass ratio of such a subpopulation. We find evidence for the existence of such a subpopulation below mass ratio q of $0.59_{-0.23}^{+0.18}$. Assuming that this subpopulation does indeed correspond to a population

of 2G+1G BBHs, we measure the fraction and merger rate of hierarchical mergers in the BBH population. We also characterize the resultant $q-\chi_1$ correlation in the overall BBH population, and describe how it naturally leads to the observed correlation between effective spin and mass ratio (T. A. Callister et al. 2021; The LIGO Scientific Collaboration et al. 2025).

This paper is structured as follows. In Section 2, we provide a description of the phenomenological model used in the work, along with the astrophysical reasoning behind our parametrization. Section 3 describes results from our population fits, and Section 4 describes the implications of our results for the correlation between mass ratio and effective spin. We end with a summary and discussion in Section 5. The appendices contains a detailed description of our model along with result validation studies and additional figures. Throughout the paper, we use the Planck 2015 cosmology (Planck Collaboration et al. 2016) as defined in LAL (LIGO Scientific Collaboration et al. 2018). All results are quoted as 90% credible intervals.

2. MODEL SUMMARY

We wish to write down a model that exploits the robustness of predictions for hierarchical mergers as an anchor to search for such a subpopulation in the data. In what follows, we will describe the spin magnitude, spin tilt, and mass ratio expectations for hierarchical mergers, and use these to motivate a model to search for them. Although our model is motivated by theoretical arguments, it does allow for the *absence* of a hierarchical subpopulation. As we will show in Section 3, we find consistent evidence for such a subpopulation in the data.

2.1. Astrophysical motivation

When two BHs merge, angular momentum conservation dictates that the final remnant BH acquires the combined spin angular momenta of the progenitor BHs and their orbital angular momentum, after accounting for the angular momentum carried away by gravitational wave (GW) emission during the merger process. While a rough estimate of the final spin can be obtained using a Newtonian treatment (e.g. A. Buonanno et al. 2008), precise estimates of the remnant spin are only possible through numerical simulations (e.g., M. A. Scheel et al. 2009) and fitting formulae built from them (e.g., V. Varma et al. 2019). One robust prediction is that the remnant spins of BBHs having $q \gtrsim 0.5$ peak near spin magnitude of ≈ 0.69 (E. Berti & M. Volonteri 2008; F. Hofmann et al. 2016; M. Fishbach et al. 2017; D. Gerosa & E. Berti 2017; C. L. Rodriguez et al. 2019; D. Gerosa

& M. Fishbach 2021) regardless of the initial spin distribution.

In dense stellar clusters, BBHs are assembled through dynamical interactions rather than processes involving isolated binary stars. Due to the random nature of these interactions, they break any initially existing symmetry or preferential alignment between the spin angular momenta of the black holes and the orbital angular momentum. Thus, it is expected that the spin directions of *all* BBHs in a cluster, including those that are hierarchically merged, would be oriented isotropically i.e., would have no preferred direction (C. L. Rodriguez et al. 2016)².

Another process that is dynamically important in dense star clusters is mass segregation. Mass segregation drives the more massive BHs toward the cluster core. Owing to the high central density, these BHs experience frequent dynamical encounters, typically forming binaries that merge with mass ratios close to unity ($q \approx 1$) for 1G+1G mergers (e.g., L. Spitzer 1987; D. Heggie & P. Hut 2003; C. L. Rodriguez et al. 2018). If the recoil kick imparted to the remnant 2G BH is smaller than the cluster's escape velocity, the remnant remains bound near the center. Having formed from two of the most massive BHs in the cluster, the 2G BH becomes the most massive object in its vicinity and is therefore the most dynamically-active and is likely to merge with a 1G BH before another 2G BH is formed. Thus, the resultant mass ratio of the mergers will lie around $q \approx 0.5$ (C. L. Rodriguez et al. 2019; F. Antonini et al. 2019). The mass ratio distribution could be different in more massive clusters where 1G+1G merger timescales are shorter (C. L. Rodriguez et al. 2019).

To illustrate this, we plot the dataset of BBH mergers from the CMC catalog (K. Kremer et al. 2020) split by their generation in Figure 1. We also plot the histogram of mass ratios of these mergers. As is evident, most 2G+1G black holes prefer having unequal masses, with their mass ratio distribution peaking around $q \approx 0.5$. Another trend worth noting is that 1G+1G BHs dominate the total observed population above $q \gtrsim 0.6$. Thus, if we want to search for a 2G+1G population in the data, one way would be to look for a transition mass ratio below which the spin distribution has at least some support for primary spins around 0.69 and isotropic spin tilts.

2.2. Model

To investigate the features described in the preceding section, we employ a phenomenological population

² See F. Kiroğlu et al. (2025) for one example of when BBHs in star clusters can retain preferential alignment.

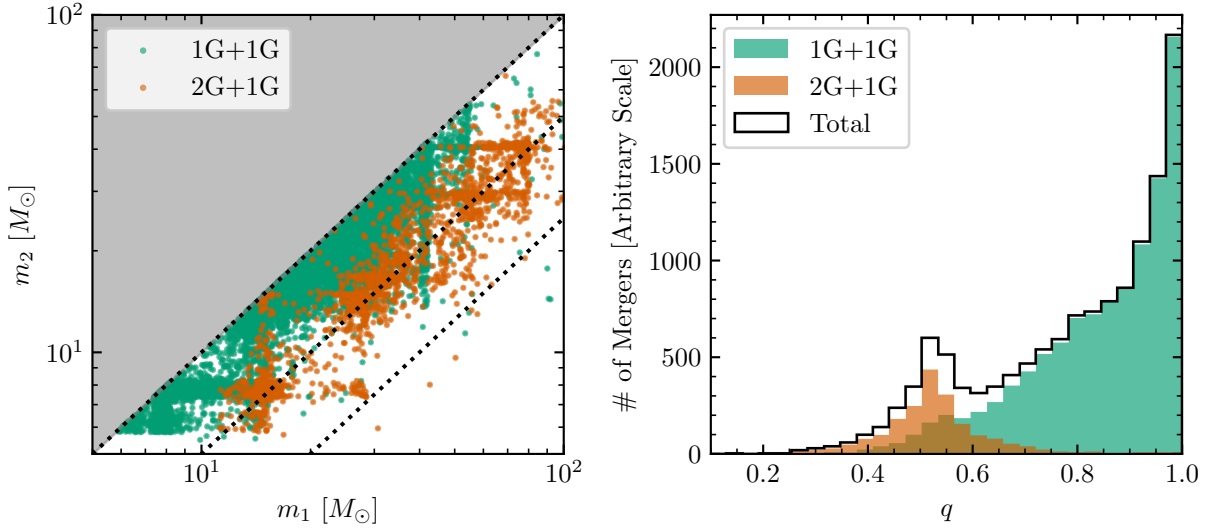


Figure 1. Predictions of 1G+1G and 2G+1G BBH mergers from the Cluster Monte Carlo simulations of dense star clusters (K. Kremer et al. 2020). The plot on the left shows BBH mergers in the m_1 - m_2 plane, where the 2G+1G mergers occupy a region where masses are unequal while 1G+1G mergers occupy the region near equal masses. This is also borne out in the mass ratio distribution of mergers plotted in the right panel, where the mass ratio distribution of 2G+1G mergers peaks at $q \approx 0.5$ whereas that of 1G+1G mergers peaks at $q \approx 1$.

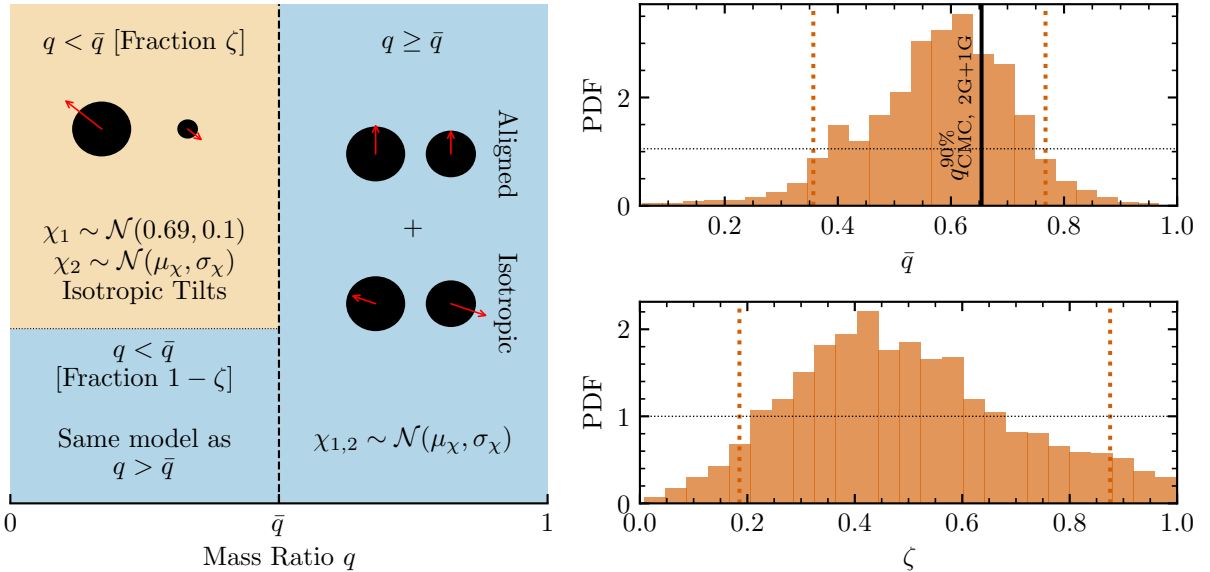


Figure 2. The left panel shows a visual summary of how our phenomenological model is constructed and parameterized. The mass ratio scale \bar{q} forms a threshold below which a fraction ζ of the population is composed of hierarchical (2G+1G) mergers. The two panels on the right show the measurements of \bar{q} and ζ using the latest catalog of GW signals. In both these panels, the horizontal gray dotted lines denote the prior on each parameter, whereas the vertical red dotted lines denote the 90% credible region of the posterior. We obtain $\bar{q} = 0.59_{-0.23}^{+0.18}$, with $\zeta = 19\text{--}88\%$ of the population below \bar{q} belonging to the hierarchically-merged population. For reference, we also plot the 90% upper limit of the 2G+1G mass ratio distribution $q_{\text{CMC, 2G+1G}}^{90\%} = 0.65$ from the CMC simulations as a vertical black solid line.

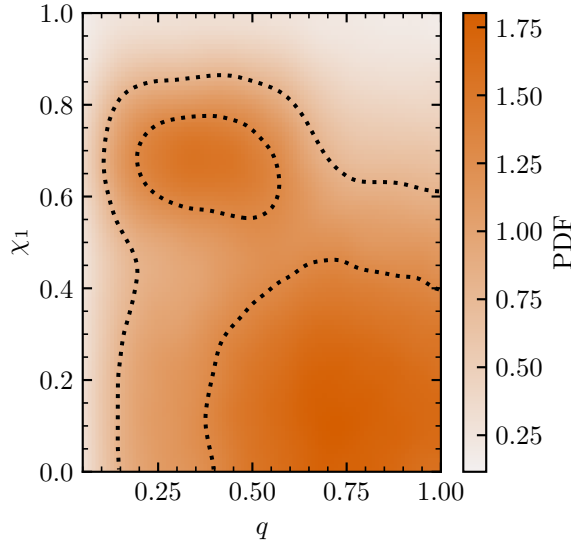


Figure 3. Smoothed histogram of fair draws from the inferred population in the spin magnitude–mass ratio plane. Two clear regions emerge in this plot: a lower-spin population concentrated towards $q \approx 1$, as well as a $\chi_1 \approx 0.7$ population concentrated around $q \approx 0.5$. Thus, there is an apparent anti-correlation between the primary spin magnitude and mass ratio.

model. For the primary mass distribution, we adopt the BROKEN POWER LAW + TWO PEAKS mass model used in the [The LIGO Scientific Collaboration et al. \(2025\)](#), but also allowing for a maximum secondary mass as done in [H. Tong et al. \(2025b\)](#). We introduce a mass ratio threshold \bar{q} that forms the dividing line between two subpopulations that differ in their spin distributions. For binaries with $q \geq \bar{q}$, we utilize the spin distribution models from [The LIGO Scientific Collaboration et al. \(2025\)](#), parameterizing spin magnitudes as a normal distribution with mean μ_χ and width σ_χ truncated to the physical range $[0, 1]$. Spin tilts in this regime are allowed to have an isotropic component as well as a component parameterizing preferential alignment. For $q < \bar{q}$, we posit that a fraction ζ of the population follows an isotropic spin distribution with primary spin magnitudes consistent with hierarchical mergers, i.e., a truncated normal distribution with mean 0.69 and width 0.1. While this is a strong prior choice, we show in Appendix B that varying the width does not affect the inference from the model significantly. The secondary spin distribution follows the spin magnitudes in the main population. The rest of the mergers (fraction $1 - \zeta$) in the $q < \bar{q}$ population follow the same spin distribution as the $q \geq \bar{q}$ population.

A schematic visualization of the model is provided in the left panel of Figure 2, and a more detailed description of the model can be found in Appendix A.

3. RESULTS

Using a hierarchical Bayesian inference framework ([T. J. Loredo 2004](#); [E. Thrane & C. Talbot 2019](#); [S. Vitale et al. 2022](#)), we fit the model described in Section 2.2 to GWTC-4 data. We use the same dataset as used in the LVK Collaboration’s analysis of GWTC-4 ([The LIGO Scientific Collaboration et al. 2025](#)), but with two changes:

1. We exclude the massive event GW231123 ([A. G. Abac et al. 2025b](#)) from the dataset.
2. We include the events GW241011 and GW241110 ([A. G. Abac et al. 2025a](#)) released from the second half of observing run 4 (O4). These events have been proposed to be consistent with hierarchical origin ([A. G. Abac et al. 2025a](#)).

While this forms our default dataset, our results do not change significantly either by adding GW231123 or leaving out GW241011 and GW241110. Consistency checks leaving out the latter can be found in Appendix B. To model the sensitivity of the GW detectors and correct for selection effects, we use the injection campaign from [R. Essick et al. \(2025\)](#). We use the GWPOPULATION ([C. Talbot et al. 2025](#)), GWPOPULATION_PIPE ([C. Talbot 2021](#)), and BILBY software packages for our inference, sampling the posterior with the nested sampler implemented in the DYNESTY software package ([J. S. Speagle 2020](#)).

The main population parameters of interest are \bar{q} and ζ . We find that a model with a transition in spins at \bar{q} is preferred over a model where there is no such transition by a Bayes factor of ≈ 15 . The right panel of Figure 2 shows the results from this model. We measure $\bar{q} = 0.59^{+0.18}_{-0.23}$, implying that the putative hierarchically-merged population prefers asymmetric masses below this mass ratio scale. This result is consistent with expectations from the CMC simulation suite, which predicts a 90% upper limit of $q = 0.65$ for the 2G+1G population averaged across cluster masses, metallicities, and virial radii. Furthermore, we infer that $\zeta = 19.88\%$ (90% credible interval) of the population below \bar{q} is composed of the putative hierarchically-merged subpopulation, corresponding to a merger rate at redshift $z = 0.2$ of $1.6^{+3.3}_{-1.4} \text{ Gpc}^{-3} \text{ yr}^{-1}$. This inferred merger rate is consistent with the lower limit of the 2G+1G merger rate inferred in [H. Tong et al. \(2025b\)](#), as well as the 2G+1G merger rates inferred [H. Tong et al. \(2025a\)](#) and [A. M. Farah et al. \(in prep.\)](#). In Appendix B, we explore

the effects of Monte Carlo uncertainty thresholds on our results.

Assuming a scaling of ≈ 7.5 between the 2G+1G rate and the total merger rate in dense clusters (i.e. 1G+1G and all hierarchical mergers), consistent with predictions from CMC simulations (e.g. A. Mai et al. 2025), we find that a median of 40% of all binaries merge in dense star clusters. However, this quantity is not constrained precisely, with the 90% credible region being 5-100%.

To further visualize our results, we plot the density of 10^5 fair draws from the population in the $q-\chi_1$ plane in Figure 3. In this plane, the separation between the two populations is clearly visible. Near $q \approx 1$, most mergers have low spins, with many having spins consistent with zero. On the other hand, the region with $q \lesssim 0.6$ is dominated by primary spins centered around 0.69. This effectively showcases the correlation in the $q-\chi_1$ plane—mergers with highly-spinning primaries consistent with hierarchical mergers prefer to lie at unequal masses when compared to those inconsistent with hierarchical mergers.

4. CONSEQUENCES FOR THE CORRELATION BETWEEN EFFECTIVE INSPIRAL SPIN AND MASS RATIO

The effective inspiral spin χ_{eff} is defined as the mass-weighted sum of component spin vectors $\vec{\chi}_1$ and $\vec{\chi}_2$ aligned along the direction of the orbital angular momentum \vec{L}_{orb} . That is,

$$\chi_{\text{eff}} = \frac{m_1 \vec{\chi}_1 + m_2 \vec{\chi}_2}{m_1 + m_2} \cdot \vec{L}_{\text{orb}}. \quad (1)$$

The effective inspiral spin is approximately conserved during the inspiral of a BBH and it encodes the leading-order dependence of the component spins on the orbit and consequently on the GW signal emanating from the system (T. Damour 2001; É. Racine 2008; P. Ajith et al. 2011). At the population-level, a correlation between the q and χ_{eff} has been known since the work of T. A. Callister et al. (2021) who found that, when the χ_{eff} distribution is modeled as a Gaussian at each q value, the *mean* of the χ_{eff} distribution decreases with increasing q . More recently, it was found that either the *mean* or the *width* of the χ_{eff} distribution can vary as a function of q (The LIGO Scientific Collaboration et al. 2025), with there being preference for the distribution narrowing as a function of q . We find that this latter result follows naturally from our inference of the $q-\chi_1$ correlation.

For each posterior sample of our population parameters, we generate 10^4 fair draws from the population of masses and spins. We convert the spins to χ_{eff} and plot the first two cumulants i.e., the mean $\mu_{\chi_{\text{eff}}}$ and

width (standard deviation) $\sigma_{\chi_{\text{eff}}}$ of the χ_{eff} samples as a function of mass ratio. We do not make the assumption that the χ_{eff} distribution is Gaussian distributed in each q bin—in fact, this is not generally true in our model at all values of q since the . The results are plotted in Figure 4. The left panel shows $\mu_{\chi_{\text{eff}}}$ as a function of mass ratio. This quantity is not visibly correlated with the mass ratio, and hovers around zero across the entire range of q . On the other hand, $\sigma_{\chi_{\text{eff}}}$ is correlated with q —the width of the χ_{eff} distribution narrows as a function of q . The $\sigma_{\chi_{\text{eff}}}-q$ correlation is not linear throughout the entire mass ratio space, but rather is composed of an approximately constant behavior above $q \approx 0.7$ and a linear curve with slope of ≈ -0.2 below $q \approx 0.7$. This correlation is a direct consequence of the $q-\chi_1$ anti-correlation in Figure 3, coupled with the isotropic spin distribution assumed for the low- q population. Taken at face value, these results suggest that using a linear model for correlations between the mean and width of the χ_{eff} distribution and q perhaps amount to model mis-specification, and future analyses should concentrate on more flexible parametric models or non-parametric models (C. Adamcewicz & E. Thrane 2022; C. Adamcewicz et al. 2023; J. Heinzel et al. 2025; A. Ray et al. 2025) to capture the correlation.

5. DISCUSSION

In this work, we used robust predictions for the spins of hierarchically-merged second-generation black holes to characterize their subpopulation in the distribution of BBH masses and spins. We found that such a subpopulation lies below a mass ratio of $\bar{q} = 0.59_{-0.23}^{+0.18}$, and could compose 19-88% of the population in this region. Our work adds to the growing evidence of hierarchical mergers in GW data (C. Kimball et al. 2020, 2021; G. Pierra et al. 2024; Y.-J. Li et al. 2024, 2025a; F. Antonini et al. 2025a,b; H. Tong et al. 2025a; S. Banagiri et al. 2025; E. Berti et al. 2025; S. Afroz & S. Mukherjee 2025; A. M. Farah et al. in prep.) and provides estimates of the 2G+1G merger rates consistent with these works. These results imply the existence of an anti-correlation in the $q-\chi_1$ plane, and naturally predict the narrowing of the χ_{eff} distribution with mass ratio. The approach used here also does not explicitly model the hierarchical primary mass distribution differently from rest of the population, although e.g., 2G+1G mergers past $m_2 \approx 45 \text{ M}_\odot$ cutoff (H. Tong et al. 2025b; F. Antonini et al. 2025a) are implicitly accounted for through the q -dependence of the χ_1 distribution. In a companion paper (A. M. Farah et al. in prep.), we account for different mass distributions for these subpopulations and show that 2G+1G mergers likely have a merger rate

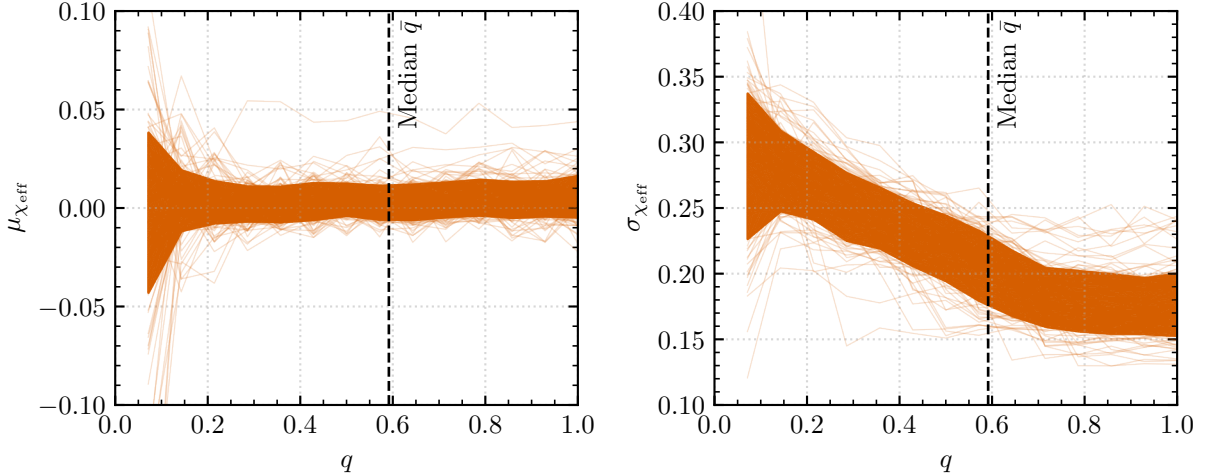


Figure 4. Mean $\mu_{\chi_{\text{eff}}}$ and width $\sigma_{\chi_{\text{eff}}}$ of the χ_{eff} distribution inferred from our model as a function of mass ratio q .

that evolves more steeply with redshift as compared to the rest of the population, thereby providing a potential explanation for the observed broadening of the χ_{eff} distribution with redshift (S. Biscoveanu et al. 2022; The LIGO Scientific Collaboration et al. 2025). Taken together with results of this work, a promising picture involving hierarchical mergers to explain various observed correlations in the BBH population is emerging. While we use a strongly-modeled approach for the BBH population in this work, it should be straightforward to verify our results using the many weakly-modeled approaches suggested in the literature (J. Godfrey et al. 2023; J. Heinzel et al. 2025; A. Ray et al. 2025; V. Tiwari 2025).

Several previous studies have also searched for subpopulations of hierarchical mergers using phenomenological models. Many of these make use of more sophisticated and self-consistent models (e.g. Z. Doctor et al. 2020; C. Kimball et al. 2020, 2021; M. Mould et al. 2022; Y.-Z. Wang et al. 2022). Our approach is different as it chooses to anchor the hierarchical subpopulation to a single and highly robust theoretical prediction. In spirit, our approach is most similar to that presented in V. Baibhav et al. (2023), which looks for separate dynamical and isolated channels through spin orientations, but does not explicitly apply their methodology to search for hierarchical mergers. This work also assumes that the hierarchical merger subpopulation has isotropic spin tilts; indeed A. M. Farah et al. (in prep.) finds that the spin tilt distribution of such a subpopulation is consistent with being isotropic. We also note that some studies (Y.-J. Li et al. 2025b; A. Hussain et al. 2026) identify an aligned, highly-spinning subpopulation of BBHs, which has been proposed as an explanation for the observed variation in the mean of the χ_{eff} distribution with q (Y.-J. Li et al. 2025b). How-

ever, this subpopulation is characterized predominantly by spin magnitudes $\gtrsim 0.8$ and is not explicitly targeted by the population model in this work.

The methods used in this paper and its companion (A. M. Farah et al. in prep.) essentially isolate the hierarchically-merged subpopulation from the rest of the population. Assuming that these hierarchical mergers take place in dense star clusters, one can use these to learn about their properties, especially at high redshift where one cannot access these clusters electromagnetically. For example, the BBH mass distribution and evolution of the merger rate with redshift can be used to study the mass, radius, escape velocity, and metallicity distribution of dense clusters in the Universe (M. Fishbach & G. Fragione 2023). Furthermore, a robust prediction from models of dense star clusters is the existence of eccentric BBH mergers (e.g. C. L. Rodriguez et al. 2018; M. Zevin et al. 2021; A. Vijaykumar et al. 2024) making up a few per cent of the total population from dense star clusters. This suggests that the hints of eccentric mergers (e.g. I. Romero-Shaw et al. 2022; N. Gupte et al. 2025) found in GW data are not surprising.

Looking ahead, data from the rest of LVK’s fourth observing run is expected to increase the total number of BBHs by a factor of 2 (B. P. Abbott et al. 2018). This will allow for a deeper characterization of the subpopulation of 2G+1G mergers, and more precise constraints on the merger rate of such systems.

ACKNOWLEDGEMENTS

We would like to thank Sourav Chatterjee, Thomas Dent, Ish Gupta, Daniel Holz, Kyle Kremer, Utkarsh Mali, Gregoire Pierra, Hui Tong, and Mike Zevin for many useful conversations. We extend special thanks to

Bart Ripperda for granting us access to the BEE workstation at CITA, where the computations for this work were performed.

AV acknowledges support from the Natural Sciences and Engineering Research Council of Canada (NSERC) (funding reference number 568580). MF acknowledges support from the NSERC under grant RGPIN-2023-05511, the Alfred P. Sloan Foundation, and the Ontario Early Researcher Award. This material is based upon work supported by NSF's LIGO Laboratory which is a major facility fully funded by the National Science Foundation. This research was supported in part by grant NSF PHY-2309135 to the Kavli Institute for Theoretical Physics (KITP).

Software: This work made use of the following software packages: `astropy` (Astropy Collaboration et al. 2013, 2018, 2022), `Jupyter` (F. Perez & B. E. Granger

2007; T. Kluyver et al. 2016), `matplotlib` (J. D. Hunter 2007), `numpy` (C. R. Harris et al. 2020), `pandas` (Wes McKinney 2010; T. pandas development team 2025), `python` (G. Van Rossum & F. L. Drake 2009), `scipy` (P. Virtanen et al. 2020; R. Gommers et al. 2025), `Bilby` (G. Ashton et al. 2019; I. M. Romero-Shaw et al. 2020; C. Talbot et al. 2025), `corner.py` (D. Foreman-Mackey 2016; D. Foreman-Mackey et al. 2024), `Cython` (S. Behnel et al. 2011), `JAX` (J. Bradbury et al. 2018), and `tqdm` (C. da Costa-Luis et al. 2024), `Dynesty` (J. S. Speagle 2020), `gwpopulation` (C. Talbot et al. 2025), `gwpopulation_pipe` (C. Talbot 2021).

This research has made use of the Astrophysics Data System, funded by NASA under Cooperative Agreement 80NSSC21M00561.

Software citation information aggregated using [The Software Citation Station](#) (T. Wagg & F. S. Broekgaarden 2024; T. Wagg et al. 2025).

APPENDIX

A. MODEL DETAILS

To model the BBH population, we use the BROKEN POWER LAW + TWO PEAKS (BP2P) as our starting point. This model and its associated parameters Λ are described in the Appendix of [The LIGO Scientific Collaboration et al. \(2025\)](#). Following [H. Tong et al. \(2025b\)](#), we modify the mass ratio q distribution to account for a cutoff/gap m_{thresh} in secondary masses. The mass model can be written as,

$$\pi(m_1, q | \Lambda) = \text{BP2P}(m_1 | \Lambda) \pi(q | m_1, \Lambda) ; \quad \pi(q | m_1, \Lambda) = \begin{cases} 0 & \text{if } m_1 q > m_{\text{thresh}} \\ q^{\beta_q} & \text{otherwise} \end{cases} \quad (\text{A1})$$

To parameterize the distribution of spin magnitudes and cosine of the tilt angles ($\cos \theta_1$ and $\cos \theta_2$ for the primary and secondary respectively), we define a mass ratio scale \bar{q} that separates the hierarchical subpopulation from the rest of the population.

$$\pi(\chi_1, \chi_2, \cos \theta_1, \cos \theta_2 | q, \Lambda) = \Theta[q < \bar{q}] \left\{ \zeta \frac{\mathcal{N}_{[0,1]}^{\chi_1}(0.69, 0.1) \mathcal{N}_{[0,1]}^{\chi_2}(\mu_\chi, \sigma_\chi)}{4} + (1 - \zeta) \pi_{\text{default}}(\chi_1, \chi_2, \cos \theta_1, \cos \theta_2 | \Lambda) \right\} \quad (\text{A2})$$

$$+ \Theta[q \geq \bar{q}] \{ \pi_{\text{default}}(\chi_1, \chi_2, \cos \theta_1, \cos \theta_2 | \Lambda) \}. \quad (\text{A3})$$

Here, π_{default} is given by,

$$\pi_{\text{default}}(\chi_1, \chi_2, \cos \theta_1, \cos \theta_2 | \Lambda) = \mathcal{N}_{[0,1]}^{\chi_1}(\mu_\chi, \sigma_\chi) \mathcal{N}_{[0,1]}^{\chi_2}(\mu_\chi, \sigma_\chi) \left\{ \frac{\xi}{4} + (1 - \xi) \mathcal{N}_{[-1,1]}^{\cos \theta_1}(\mu_t, \sigma_t) \mathcal{N}_{[-1,1]}^{\cos \theta_2}(\mu_t, \sigma_t) \right\} \quad (\text{A4})$$

where $\mathcal{N}_{[x_1, x_2]}^x(\mu, \sigma)$ denotes a normal distribution in x with mean μ and standard deviation σ truncated between x_1 and x_2 . The full model can be written as,

$$\pi(m_1, q, \chi_1, \chi_2, \cos \theta_1, \cos \theta_2 | \Lambda) = \pi(m_1, q | \Lambda) \pi(\chi_1, \chi_2, \cos \theta_1, \cos \theta_2 | q, \Lambda). \quad (\text{A5})$$

B. VALIDATION STUDIES AND ADDITIONAL FIGURES

In this section, we present a set of validation studies examining the sensitivity of our results to the analysis choices adopted in this work, along with additional supporting figures.

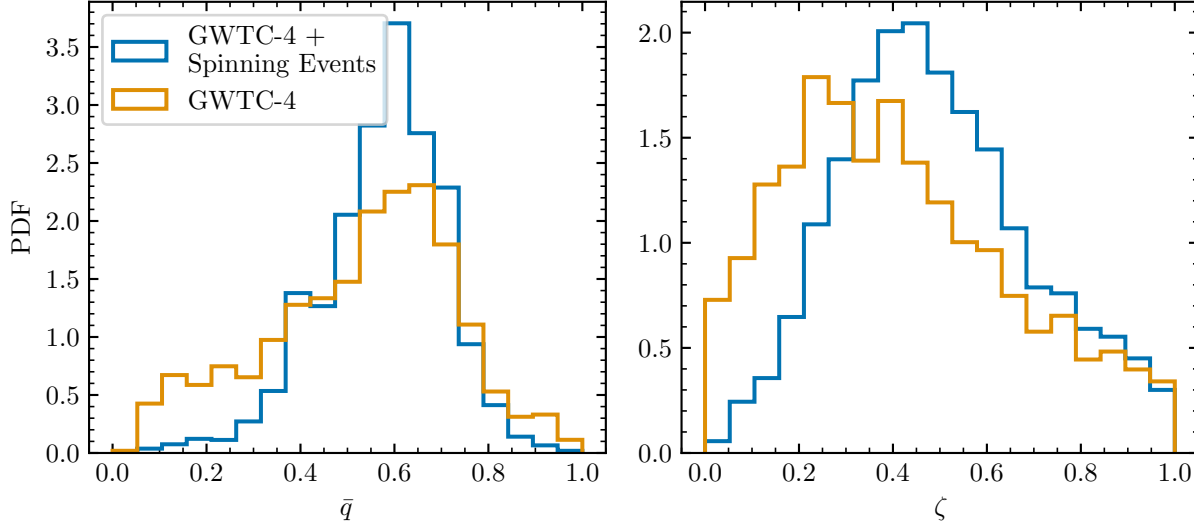


Figure 5. Comparison of \bar{q} and ζ posteriors obtained by including and excluding GW241011 and GW241110 (referred to as “Spinning Events” in the figure legend) in the population. For all results in the main text, we include GW241011 and GW241110 in our dataset.

The posterior PDFs of \bar{q} and ζ obtained with and without the inclusion of the spinning, asymmetric, and misaligned BBH mergers GW241011 and GW241110 (A. G. Abac et al. 2025a) are shown in Figure 5. As expected, the constraints on \bar{q} and ζ improve when these events are included. Notably, a non-trivial measurement of \bar{q} persists even when these events are excluded, indicating that the trend reported in this paper is already present in the GWTC-4 data. The shift of the posterior peak of ζ toward higher values upon the inclusion of GW241011 and GW241110 is also expected, as we do not self-consistently account for the sensitivity of the second half of O4 in our analysis. Finally, the apparent railing against $\zeta = 0$ in the GWTC-4-only posterior is driven by its correlation with low values of \bar{q} .

We also present results obtained by varying the width, σ_{2G} , of the 2G spin distribution in Figure 6. Our fiducial analysis assumes $\sigma_{2G} = 0.1$, with the corresponding mean fixed at 0.69. We find that the posterior distributions of \bar{q} and ζ are largely insensitive to changes in the width of the 2G spin distribution.

For the default results presented in the main text, we require the log-likelihood variance to satisfy $\sigma_{\ln \hat{\zeta}}^2(\Lambda) < 1$ (e.g., R. Essick & W. Farr 2022; C. Talbot & J. Golomb 2023). This requirement is enforced by setting the log-likelihood to $-\infty$ whenever the condition is not met. When this criterion is relaxed to $\sigma_{\ln \hat{\zeta}}^2(\Lambda) < 4$, the posterior constraints on \bar{q} and ζ tighten, as shown in Figure 7. Nevertheless, for the results presented in the main text, we adopt the more conservative choice of $\sigma_{\ln \hat{\zeta}}^2(\Lambda) < 1$.

Figure 8 shows the inferred putative 1G spin-magnitude distribution, together with the fixed 2G spin-magnitude distribution adopted in this work. While the 1G distribution peaks at low spin magnitudes, it exhibits a tail extending to spin magnitudes within the range assumed for the 2G population.

REFERENCES

- Abac, A. G., Abouelfettouh, I., Acernese, F., et al. 2025a, ApJL, 993, L21, doi: [10.3847/2041-8213/ae0d54](https://doi.org/10.3847/2041-8213/ae0d54)
- Abac, A. G., Abouelfettouh, I., Acernese, F., et al. 2025b, ApJL, 993, L25, doi: [10.3847/2041-8213/ae0c9c](https://doi.org/10.3847/2041-8213/ae0c9c)
- Abbott, B. P., Abbott, R., Abbott, T. D., et al. 2018, Living Reviews in Relativity, 21, 3, doi: [10.1007/s41114-018-0012-9](https://doi.org/10.1007/s41114-018-0012-9)
- Acernese, F., Agathos, M., Agatsuma, K., et al. 2015, Classical and Quantum Gravity, 32, 024001, doi: [10.1088/0264-9381/32/2/024001](https://doi.org/10.1088/0264-9381/32/2/024001)
- Adamcewicz, C., Lasky, P. D., & Thrane, E. 2023, ApJ, 958, 13, doi: [10.3847/1538-4357/acf763](https://doi.org/10.3847/1538-4357/acf763)
- Adamcewicz, C., & Thrane, E. 2022, MNRAS, 517, 3928, doi: [10.1093/mnras/stac2961](https://doi.org/10.1093/mnras/stac2961)
- Afroz, S., & Mukherjee, S. 2025, arXiv e-prints, arXiv:2509.09123, doi: [10.48550/arXiv.2509.09123](https://doi.org/10.48550/arXiv.2509.09123)
- Ajith, P., Hannam, M., Husa, S., et al. 2011, PhRvL, 106, 241101, doi: [10.1103/PhysRevLett.106.241101](https://doi.org/10.1103/PhysRevLett.106.241101)

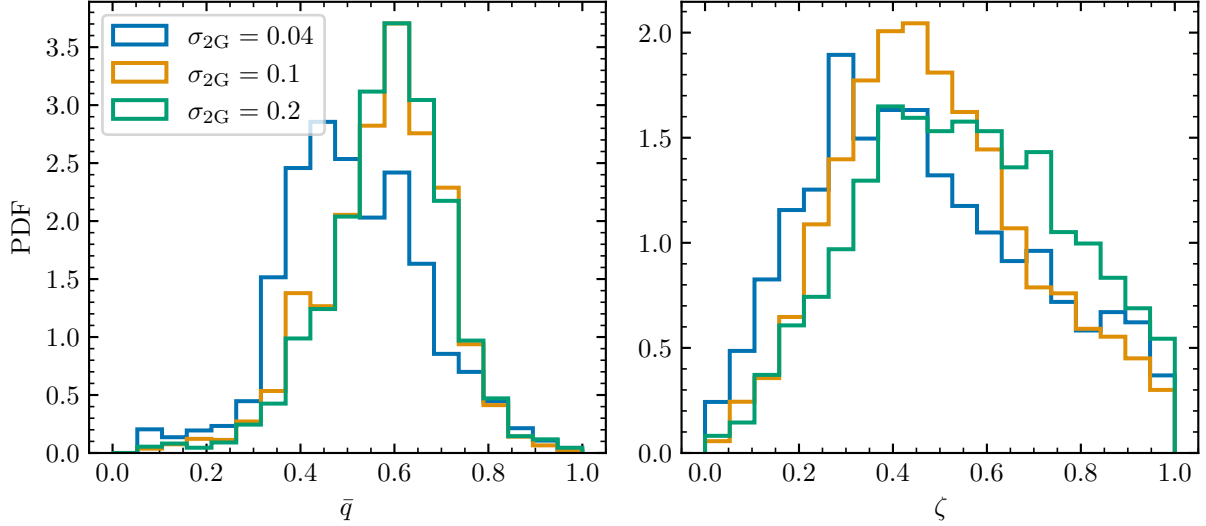


Figure 6. Comparison of \bar{q} and ζ posteriors obtained by varying widths σ_{2G} of the 2G spin distribution. The mean of the spin distribution is fixed to 0.69. For results in the main text, we fix $\sigma_{2G} = 0.1$.

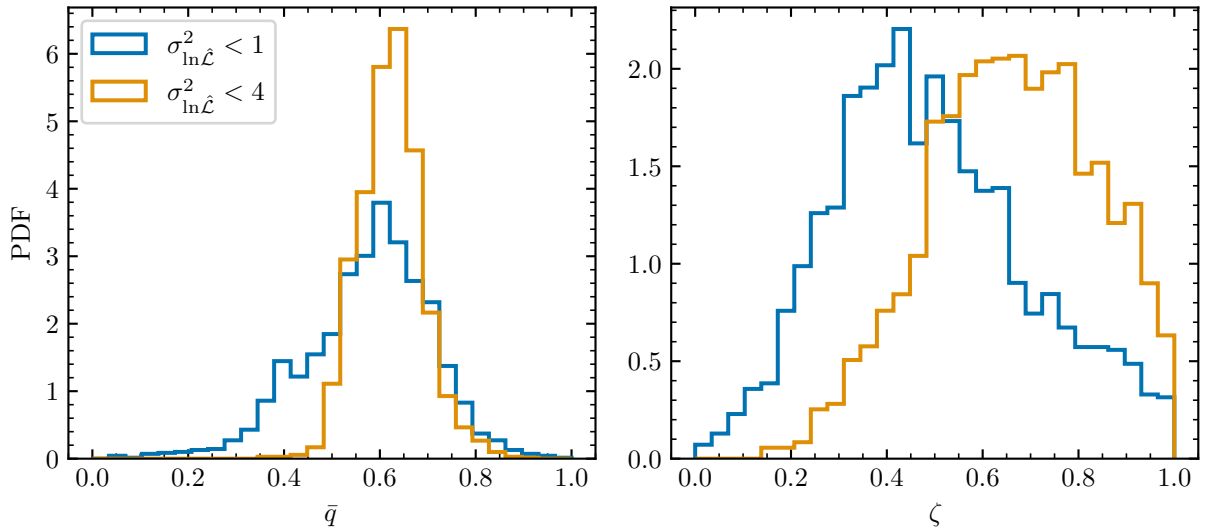


Figure 7. Comparison of \bar{q} and ζ posteriors obtained by varying the log-likelihood variance threshold. The posteriors become sharper when the default variance threshold $\sigma_{\ln \hat{L}}^2(\Lambda) < 1$ is relaxed to $\sigma_{\ln \hat{L}}^2(\Lambda) < 4$. We use the conservative choice of $\sigma_{\ln \hat{L}}^2(\Lambda) < 1$ for all results presented in the main text.

- Akutsu, T., Ando, M., Arai, K., et al. 2021, Progress of Theoretical and Experimental Physics, 2021, 05A101, doi: [10.1093/ptep/ptaa125](https://doi.org/10.1093/ptep/ptaa125)
- Antonini, F., Gieles, M., & Gualandris, A. 2019, MNRAS, 486, 5008, doi: [10.1093/mnras/stz1149](https://doi.org/10.1093/mnras/stz1149)
- Antonini, F., Romero-Shaw, I., Callister, T., et al. 2025a, arXiv e-prints, arXiv:2509.04637, doi: [10.48550/arXiv.2509.04637](https://doi.org/10.48550/arXiv.2509.04637)
- Antonini, F., Romero-Shaw, I. M., & Callister, T. 2025b, PhRvL, 134, 011401, doi: [10.1103/PhysRevLett.134.011401](https://doi.org/10.1103/PhysRevLett.134.011401)

- Ashton, G., Hübner, M., Lasky, P. D., et al. 2019, ApJS, 241, 27, doi: [10.3847/1538-4365/ab06fc](https://doi.org/10.3847/1538-4365/ab06fc)
- Astropy Collaboration, Robitaille, T. P., Tollerud, E. J., et al. 2013, A&A, 558, A33, doi: [10.1051/0004-6361/201322068](https://doi.org/10.1051/0004-6361/201322068)
- Astropy Collaboration, Price-Whelan, A. M., Sipőcz, B. M., et al. 2018, AJ, 156, 123, doi: [10.3847/1538-3881/aabc4f](https://doi.org/10.3847/1538-3881/aabc4f)
- Astropy Collaboration, Price-Whelan, A. M., Lim, P. L., et al. 2022, ApJ, 935, 167, doi: [10.3847/1538-4357/ac7c74](https://doi.org/10.3847/1538-4357/ac7c74)
- Baibhav, V., Doctor, Z., & Kalogera, V. 2023, ApJ, 946, 50, doi: [10.3847/1538-4357/acbf4c](https://doi.org/10.3847/1538-4357/acbf4c)

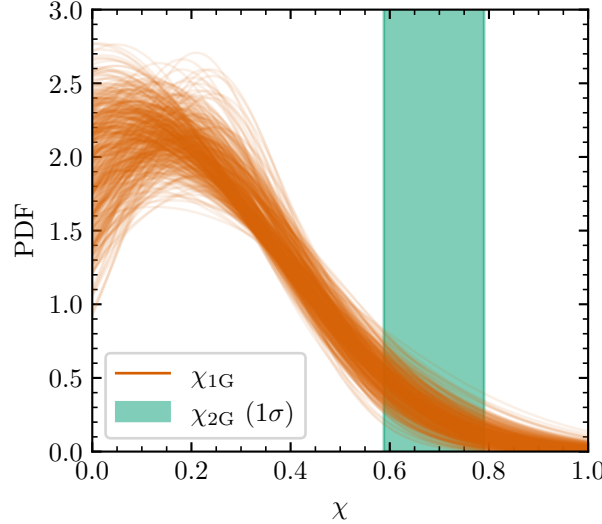


Figure 8. Inferred spin magnitude distribution for the putative 1G black holes plotted in red traces. The green shaded region encodes the the 1σ (68%) region of the 2G spin distribution (normal distribution with mean 0.69 and width 0.1 truncated between 0 and 1).

- Banagiri, S., Thrane, E., & Lasky, P. D. 2025, arXiv e-prints, arXiv:2509.15646, doi: [10.48550/arXiv.2509.15646](https://doi.org/10.48550/arXiv.2509.15646)
- Behnel, S., Bradshaw, R., Citro, C., et al. 2011, Computing in Science Engineering, 13, 31, doi: [10.1109/MCSE.2010.118](https://doi.org/10.1109/MCSE.2010.118)
- Berti, E., Cressimbeni, F., Franciolini, G., et al. 2025, arXiv e-prints, arXiv:2512.03152, doi: [10.48550/arXiv.2512.03152](https://doi.org/10.48550/arXiv.2512.03152)
- Berti, E., & Volonteri, M. 2008, ApJ, 684, 822, doi: [10.1086/590379](https://doi.org/10.1086/590379)
- Biscoveanu, S., Callister, T. A., Haster, C.-J., et al. 2022, ApJL, 932, L19, doi: [10.3847/2041-8213/ac71a8](https://doi.org/10.3847/2041-8213/ac71a8)
- Bradbury, J., Frostig, R., Hawkins, P., et al. 2018, JAX: composable transformations of Python+NumPy programs, 0.3.13 <http://github.com/google/jax>
- Buonanno, A., Kidder, L. E., & Lehner, L. 2008, PhRvD, 77, 026004, doi: [10.1103/PhysRevD.77.026004](https://doi.org/10.1103/PhysRevD.77.026004)
- Callister, T. A., Haster, C.-J., Ng, K. K. Y., Vitale, S., & Farr, W. M. 2021, ApJL, 922, L5, doi: [10.3847/2041-8213/ac2ccc](https://doi.org/10.3847/2041-8213/ac2ccc)
- da Costa-Luis, C., Larroque, S. K., Altendorf, K., et al. 2024, tqdm: A fast, Extensible Progress Bar for Python and CLI, v4.67.1 Zenodo, doi: [10.5281/zenodo.14231923](https://doi.org/10.5281/zenodo.14231923)
- Damour, T. 2001, PhRvD, 64, 124013, doi: [10.1103/PhysRevD.64.124013](https://doi.org/10.1103/PhysRevD.64.124013)
- Doctor, Z., Wysocki, D., O'Shaughnessy, R., Holz, D. E., & Farr, B. 2020, ApJ, 893, 35, doi: [10.3847/1538-4357/ab7fac](https://doi.org/10.3847/1538-4357/ab7fac)
- Essick, R., & Farr, W. 2022, arXiv e-prints, arXiv:2204.00461, doi: [10.48550/arXiv.2204.00461](https://doi.org/10.48550/arXiv.2204.00461)
- Essick, R., Coughlin, M. W., Zevin, M., et al. 2025, PhRvD, 112, 102001, doi: [10.1103/44x3-hv3y](https://doi.org/10.1103/44x3-hv3y)
- Farah, A. M., Vijaykumar, A., & Fishbach, M. in prep., Fishbach, M., & Fragione, G. 2023, MNRAS, 522, 5546, doi: [10.1093/mnras/stad1364](https://doi.org/10.1093/mnras/stad1364)
- Fishbach, M., Holz, D. E., & Farr, B. 2017, ApJL, 840, L24, doi: [10.3847/2041-8213/aa7045](https://doi.org/10.3847/2041-8213/aa7045)
- Foreman-Mackey, D. 2016, The Journal of Open Source Software, 1, 24, doi: [10.21105/joss.00024](https://doi.org/10.21105/joss.00024)
- Foreman-Mackey, D., Price-Whelan, A., Vousden, W., et al. 2024, dfm/corner.py: v2.2.3, v2.2.3 Zenodo, doi: [10.5281/zenodo.14209694](https://doi.org/10.5281/zenodo.14209694)
- Gerosa, D., & Berti, E. 2017, PhRvD, 95, 124046, doi: [10.1103/PhysRevD.95.124046](https://doi.org/10.1103/PhysRevD.95.124046)
- Gerosa, D., & Fishbach, M. 2021, Nature Astronomy, 5, 749, doi: [10.1038/s41550-021-01398-w](https://doi.org/10.1038/s41550-021-01398-w)
- Godfrey, J., Edelman, B., & Farr, B. 2023, arXiv e-prints, arXiv:2304.01288, doi: [10.48550/arXiv.2304.01288](https://doi.org/10.48550/arXiv.2304.01288)
- Gommers, R., Virtanen, P., Haberland, M., et al. 2025, scipy/scipy: SciPy 1.17.0rc1, v1.17.0rc1 Zenodo, doi: [10.5281/zenodo.17873309](https://doi.org/10.5281/zenodo.17873309)
- Gupte, N., Ramos-Buades, A., Buonanno, A., et al. 2025, PhRvD, 112, 104045, doi: [10.1103/vpyp-nvfp](https://doi.org/10.1103/vpyp-nvfp)
- Harris, C. R., Millman, K. J., van der Walt, S. J., et al. 2020, Nature, 585, 357, doi: [10.1038/s41586-020-2649-2](https://doi.org/10.1038/s41586-020-2649-2)
- Heggie, D., & Hut, P. 2003, The Gravitational Million-Body Problem: A Multidisciplinary Approach to Star Cluster Dynamics

- Heinzel, J., Mould, M., Álvarez-López, S., & Vitale, S. 2025, *PhRvD*, 111, 063043, doi: [10.1103/PhysRevD.111.063043](https://doi.org/10.1103/PhysRevD.111.063043)
- Hofmann, F., Barausse, E., & Rezzolla, L. 2016, *ApJL*, 825, L19, doi: [10.3847/2041-8205/825/2/L19](https://doi.org/10.3847/2041-8205/825/2/L19)
- Hunter, J. D. 2007, *Computing in Science & Engineering*, 9, 90, doi: [10.1109/MCSE.2007.55](https://doi.org/10.1109/MCSE.2007.55)
- Hussain, A., Isi, M., & Zimmerman, A. 2026, *ApJ*, 996, 71, doi: [10.3847/1538-4357/ae1574](https://doi.org/10.3847/1538-4357/ae1574)
- Kimball, C., Talbot, C., Berry, C. P. L., et al. 2020, *ApJ*, 900, 177, doi: [10.3847/1538-4357/aba518](https://doi.org/10.3847/1538-4357/aba518)
- Kimball, C., Talbot, C., Berry, C. P. L., et al. 2021, *ApJL*, 915, L35, doi: [10.3847/2041-8213/ac0aef](https://doi.org/10.3847/2041-8213/ac0aef)
- Kiroglu, F., Lombardi, J. C., Kremer, K., Vanderzyden, H. D., & Rasio, F. A. 2025, *ApJL*, 983, L9, doi: [10.3847/2041-8213/adc263](https://doi.org/10.3847/2041-8213/adc263)
- Kluyver, T., Ragan-Kelley, B., Pérez, F., et al. 2016, in *Positioning and Power in Academic Publishing: Players, Agents and Agendas*, ed. F. Loizides & B. Schmidt, IOS Press, 87 – 90
- Kremer, K., Ye, C. S., Rui, N. Z., et al. 2020, *ApJS*, 247, 48, doi: [10.3847/1538-4365/ab7919](https://doi.org/10.3847/1538-4365/ab7919)
- Li, Y.-J., Wang, Y.-Z., Tang, S.-P., Chen, T., & Fan, Y.-Z. 2025a, *ApJ*, 987, 65, doi: [10.3847/1538-4357/add535](https://doi.org/10.3847/1538-4357/add535)
- Li, Y.-J., Wang, Y.-Z., Tang, S.-P., & Fan, Y.-Z. 2024, *PhRvL*, 133, 051401, doi: [10.1103/PhysRevLett.133.051401](https://doi.org/10.1103/PhysRevLett.133.051401)
- Li, Y.-J., Wang, Y.-Z., Tang, S.-P., & Fan, Y.-Z. 2025b, arXiv e-prints, arXiv:2509.23897, doi: [10.48550/arXiv.2509.23897](https://doi.org/10.48550/arXiv.2509.23897)
- LIGO Scientific Collaboration, Virgo Collaboration, & KAGRA Collaboration. 2018, LVK Algorithm Library - LALSuite,, Free software (GPL) doi: [10.7935/GT1W-FZ16](https://doi.org/10.7935/GT1W-FZ16)
- LIGO Scientific Collaboration, Aasi, J., Abbott, B. P., et al. 2015, *Classical and Quantum Gravity*, 32, 074001, doi: [10.1088/0264-9381/32/7/074001](https://doi.org/10.1088/0264-9381/32/7/074001)
- Loredo, T. J. 2004, in *American Institute of Physics Conference Series*, Vol. 735, Bayesian Inference and Maximum Entropy Methods in Science and Engineering: 24th International Workshop on Bayesian Inference and Maximum Entropy Methods in Science and Engineering, ed. R. Fischer, R. Preuss, & U. V. Toussaint (AIP), 195–206, doi: [10.1063/1.1835214](https://doi.org/10.1063/1.1835214)
- Mai, A., Kremer, K., & Kiroglu, F. 2025, arXiv e-prints, arXiv:2510.21916, doi: [10.48550/arXiv.2510.21916](https://doi.org/10.48550/arXiv.2510.21916)
- Mandel, I., & Broekgaarden, F. S. 2022, *Living Reviews in Relativity*, 25, 1, doi: [10.1007/s41114-021-00034-3](https://doi.org/10.1007/s41114-021-00034-3)
- Mandel, I., & Farmer, A. 2022, *PhR*, 955, 1, doi: [10.1016/j.physrep.2022.01.003](https://doi.org/10.1016/j.physrep.2022.01.003)
- Mapelli, M. 2020, *Frontiers in Astronomy and Space Sciences*, 7, 38, doi: [10.3389/fspas.2020.00038](https://doi.org/10.3389/fspas.2020.00038)
- Mould, M., Gerosa, D., & Taylor, S. R. 2022, *PhRvD*, 106, 103013, doi: [10.1103/PhysRevD.106.103013](https://doi.org/10.1103/PhysRevD.106.103013)
- pandas development team, T. 2025, *pandas-dev/pandas: Pandas*, v3.0.0rc1 Zenodo, doi: [10.5281/zenodo.17992932](https://doi.org/10.5281/zenodo.17992932)
- Perez, F., & Granger, B. E. 2007, *Computing in Science and Engineering*, 9, 21, doi: [10.1109/MCSE.2007.53](https://doi.org/10.1109/MCSE.2007.53)
- Pierra, G., Mastrogiovanni, S., & Perriès, S. 2024, arXiv e-prints, arXiv:2406.01679, doi: [10.48550/arXiv.2406.01679](https://doi.org/10.48550/arXiv.2406.01679)
- Planck Collaboration, Ade, P. A. R., Aghanim, N., et al. 2016, *A&A*, 594, A13, doi: [10.1051/0004-6361/201525830](https://doi.org/10.1051/0004-6361/201525830)
- Racine, É. 2008, *PhRvD*, 78, 044021, doi: [10.1103/PhysRevD.78.044021](https://doi.org/10.1103/PhysRevD.78.044021)
- Ray, A., Hernandez, I. M., Breivik, K., & Creighton, J. 2025, *ApJ*, 991, 17, doi: [10.3847/1538-4357/adf22a](https://doi.org/10.3847/1538-4357/adf22a)
- Rodriguez, C. L., Amaro-Seoane, P., Chatterjee, S., & Rasio, F. A. 2018, *PhRvL*, 120, 151101, doi: [10.1103/PhysRevLett.120.151101](https://doi.org/10.1103/PhysRevLett.120.151101)
- Rodriguez, C. L., Zevin, M., Amaro-Seoane, P., et al. 2019, *PhRvD*, 100, 043027, doi: [10.1103/PhysRevD.100.043027](https://doi.org/10.1103/PhysRevD.100.043027)
- Rodriguez, C. L., Zevin, M., Pankow, C., Kalogera, V., & Rasio, F. A. 2016, *ApJL*, 832, L2, doi: [10.3847/2041-8205/832/1/L2](https://doi.org/10.3847/2041-8205/832/1/L2)
- Romero-Shaw, I., Lasky, P. D., & Thrane, E. 2022, *ApJ*, 940, 171, doi: [10.3847/1538-4357/ac9798](https://doi.org/10.3847/1538-4357/ac9798)
- Romero-Shaw, I. M., Talbot, C., Biscoveanu, S., et al. 2020, *MNRAS*, 499, 3295, doi: [10.1093/mnras/staa2850](https://doi.org/10.1093/mnras/staa2850)
- Scheel, M. A., Boyle, M., Chu, T., et al. 2009, *PhRvD*, 79, 024003, doi: [10.1103/PhysRevD.79.024003](https://doi.org/10.1103/PhysRevD.79.024003)
- Speagle, J. S. 2020, *MNRAS*, 493, 3132, doi: [10.1093/mnras/staa278](https://doi.org/10.1093/mnras/staa278)
- Spitzer, L. 1987, *Dynamical evolution of globular clusters*
- Talbot, C. 2021, *GWPopulation pipe*, 0.3.0 Zenodo, doi: [10.5281/zenodo.5654673](https://doi.org/10.5281/zenodo.5654673)
- Talbot, C., Farah, A., Galauadage, S., Golomb, J., & Tong, H. 2025, *The Journal of Open Source Software*, 10, 7753, doi: [10.21105/joss.07753](https://doi.org/10.21105/joss.07753)
- Talbot, C., & Golomb, J. 2023, *MNRAS*, 526, 3495, doi: [10.1093/mnras/stad2968](https://doi.org/10.1093/mnras/stad2968)
- Talbot, C., Ashton, G., Hübner, M., et al. 2025, *bilby-dev/bilby*: v.2.7.1, v2.7.1 Zenodo, doi: [10.5281/zenodo.17533961](https://doi.org/10.5281/zenodo.17533961)
- The LIGO Scientific Collaboration, the Virgo Collaboration, the KAGRA Collaboration, et al. 2025, arXiv e-prints, arXiv:2508.18083, doi: [10.48550/arXiv.2508.18083](https://doi.org/10.48550/arXiv.2508.18083)
- Thrane, E., & Talbot, C. 2019, *PASA*, 36, e010, doi: [10.1017/pasa.2019.2](https://doi.org/10.1017/pasa.2019.2)

- Tiwari, V. 2025, arXiv e-prints, arXiv:2510.25579, doi: [10.48550/arXiv.2510.25579](https://doi.org/10.48550/arXiv.2510.25579)
- Tong, H., Callister, T. A., Fishbach, M., et al. 2025a, arXiv e-prints, arXiv:2511.05316, doi: [10.48550/arXiv.2511.05316](https://doi.org/10.48550/arXiv.2511.05316)
- Tong, H., Fishbach, M., Thrane, E., et al. 2025b, arXiv e-prints, arXiv:2509.04151, doi: [10.48550/arXiv.2509.04151](https://doi.org/10.48550/arXiv.2509.04151)
- Van Rossum, G., & Drake, F. L. 2009, Python 3 Reference Manual (Scotts Valley, CA: CreateSpace)
- Varma, V., Gerosa, D., Stein, L. C., Hébert, F., & Zhang, H. 2019, PhRvL, 122, 011101, doi: [10.1103/PhysRevLett.122.011101](https://doi.org/10.1103/PhysRevLett.122.011101)
- Vijaykumar, A., Hanselman, A. G., & Zevin, M. 2024, ApJ, 969, 132, doi: [10.3847/1538-4357/ad4455](https://doi.org/10.3847/1538-4357/ad4455)
- Virtanen, P., Gommers, R., Oliphant, T. E., et al. 2020, Nature Methods, 17, 261, doi: [10.1038/s41592-019-0686-2](https://doi.org/10.1038/s41592-019-0686-2)
- Vitale, S., Gerosa, D., Farr, W. M., & Taylor, S. R. 2022, in Handbook of Gravitational Wave Astronomy, ed. C. Bambi, S. Katsanevas, & K. D. Kokkotas, 45, doi: [10.1007/978-981-15-4702-7_45-1](https://doi.org/10.1007/978-981-15-4702-7_45-1)
- Wagg, T., Broekgaarden, F., Van-Lane, P., Wu, K., & Gültekin, K. 2025, TomWagg/software-citation-station: v1.4, v1.4 Zenodo, doi: [10.5281/zenodo.17654855](https://doi.org/10.5281/zenodo.17654855)
- Wagg, T., & Broekgaarden, F. S. 2024, arXiv e-prints, arXiv:2406.04405. <https://arxiv.org/abs/2406.04405>
- Wang, Y.-Z., Li, Y.-J., Vink, J. S., et al. 2022, ApJL, 941, L39, doi: [10.3847/2041-8213/aca89f](https://doi.org/10.3847/2041-8213/aca89f)
- Wes McKinney. 2010, in Proceedings of the 9th Python in Science Conference, ed. Stéfan van der Walt & Jarrod Millman, 56 – 61, doi: [10.25080/Majora-92bf1922-00a](https://doi.org/10.25080/Majora-92bf1922-00a)
- Zevin, M., Romero-Shaw, I. M., Kremer, K., Thrane, E., & Lasky, P. D. 2021, ApJL, 921, L43, doi: [10.3847/2041-8213/ac32dc](https://doi.org/10.3847/2041-8213/ac32dc)